An analytic solution for capillary thinning and breakup of FENE-P fluids

Caroline Wagner [*1], Lydia Bourouiba [†2], and Gareth McKinley [‡1]

[1]Department of Mechanical Engineering, Massachusetts Institute of Technology, Cambridge, MA. 02139

[2]Institute for Medical Engineering and Science, Department of Civil & Environmental Engineering, Massachusetts Institute of Technology, Cambridge, MA. 02139

January 19, 2015

Abstract

The FENE-P model of a fluid is particularly suitable for describing the rheology of dilute polymer solutions (Newtonian solvents containing small amounts of dissolved polymer) as a result of its ability to capture nonlinear effects arising from the finite extensibility of the polymer chains. In extensional flows, these polymer solutions exhibit dramatically different behaviour from the corresponding Newtonian solvents alone, notably through the creation of persistent filaments when stretched. By using the technique of capillary thinning to study the dynamics of the thinning process of these filaments, the transient extensional rheology of the fluid can be characterized. We show that under conditions of uniaxial elongational flow, a composite analytic solution can be developed to predict the time evolution of the radius of the filament. Furthermore we derive an analytic expression for the finite time to breakup of the fluid filaments. This breakup time agrees very well with results obtained from full numerical simulations, and both numerics and theory predict an increase in the time to breakup as the finite extensibility parameter b, related to the molecular weight of the polymer, is increased. As $b \to \infty$, the results converge to an asymptotic result for the breakup time which shows that the breakup time grows as $t_{break} \sim \ln(M_W)$, where M_W is the molecular weight of the dilute polymer solution.

[*]cewagner@mit.edu
[†]lbouro@mit.edu
[‡]gareth@mit.edu

1 Introduction

The addition of a small amount of polymer to a Newtonian solvent can yield rather dramatic differences in the behaviour of the fluid under extension due to the increased resistance to flow [1, 2]. This can readily be seen through the ability of these solutions to form persistent filaments and delay capillary breakup when stretched. This polymer-induced phenomenon has many industrial applications, including inkjet printing where minimization of satellite droplet formation is essential for printing quality [3, 4]. Additionally, in as early as 1908, Fano studied this phenomenon in the context of biopolymer solutions such as egg white, bile, and plant extracts [5]. This elasticity is vital for many of the functions that these biological fluids serve, and changes in rheological properties are sometimes used as diagnostic tools to monitor the state of the fluid in question. For instance, Kopito and Kosasky [6] performed fertility studies to assess hormone levels during the menstrual cycle by measuring the rheological properties of cervical mucus. Further, Basilevsky and coworkers have explored the degradation of sputum upon exposure to certain bacteria as measured through changes in its elastic properties [7]. As a final example, Zussman and coworkers have noted that differences in saliva viscoelasticity between teenagers and the elderly may explain why the most common dental health issues plaguing these two age groups differ [8]. Clearly, the ability to quantify the elastic properties of such fluids is essential for these types of studies.

Following the original analysis by Entov and coworkers [9, 10, 11], capillary thinning rheometry has become a standard technique for rapidly measuring the extensional properties of a wide range of viscoelastic fluids, including polymer solutions. The Capillary Breakup Extensional Rheometer (CaBER) is a commercially available instrument that is frequently used to perform these types of measurements. During a capillary thinning experiment, a small sample of fluid is stretched between two plates to form a liquid bridge, and a laser micrometer tracks the midpoint radius of the filament as it thins under the action of capillary forces. In general for dilute polymer solutions, once fluid inertia can be neglected, the filament thinning process is initially governed by a viscocapillary force balance in which viscous extensional stresses from the solvent oppose the increasing capillary pressure, and is followed by a later elastocapillary stage in which stresses generated by the stretching of the polymer chains dominate [12]. From measurements of the time evolution of the filament radius, the breakup time of the filament and relaxation time of the fluid can be obtained, both of which provide quantitative measures of the fluid's viscoelastic properties.

Entov and Hinch [11] provide a full numerical solution for the evolution in the radius of a filament of a Finitely Extensible Nonlinear Elastic (FENE) fluid undergoing uniaxial elongational flow during elastocapillary thinning. The FENE model for a polymer solution assumes a Newtonian solvent containing a dilute suspension of polymer chains that are modelled as finitely extensible (with maximum extensibility b) and non-linearly elastic. To date, CaBER analysis has typically consisted of experimental measurement and comparison with numerical simulations of filament thinning using the FENE model. Select examples include Liang and Mackley [13], who studied the concentration-dependent relaxation times of polyisobutylene (PIB) solutions, as well as Anna [14, 15] and Clasen and coworkers [16], who studied the dynamics of elastocapillary thinning in various concentrations and molecular weights of polystyrene-based Boger fluids and compared their results with numerical simulations of the FENE model to determine the effective elongational relaxation time.

As a result of the continued interest in capillary thinning rheometry, it would be useful to have an analytic solution that gives the finite time to breakup and describes the evolution in the mid-filament radius $R(t)$ as one varies the concentration, molecular weight, or solvent viscosity of a polymer solution. Recently, Torres and coworkers [17] developed an exact implicit analytic solution for the finite time to breakup and time evolution of the radius for a Giesekus fluid undergoing capillary-driven thinning. They studied semi-dilute and concentrated guar gum solutions, and because of the very viscous nature of these entangled systems, their analytic model for the forces acting on the filament was able to neglect the contributions of solvent viscosity with negligible consequence. Many biological fluids, however, are dilute polymer solutions, and in this concentration regime, the solvent viscosity is known to play an important role in the overall extensional stress response, particularly at early times [12]. Motivated by these developments, we analyse the elastocapillary thinning of a filament of a Finitely Extensible Nonlinear Elastic (FENE) fluid, paying special attention to the different phases of the process including the initial solvent response, the intermediate elastic regime when the chains are partially stretched, and the ultimate approach to maximum extensibility as the polymer chains become fully stretched.

We begin by revisiting the derivation of the FENE-P constitutive equation (where the -P indicates the Peterlin approximation) in several different forms, from which we derive an analytic expression for the time evolution of the mid-filament radius $R(t)$. Using this result, we can then determine the finite time to breakup when the polymer stress contribution is considered in isolation of the viscous solvent response.

We subsequently consider the special limit of infinite extensibility, and show via comparison with the corresponding result from Entov and Hinch [11] how the solvent viscosity must be explicitly accounted for. We ultimately present a composite analytic solution, which incorporates both an initial viscous-dominated phase and a later polymer-dominated phase. We explore the level of extensional strain at which the transition from a viscocapillary to elastocapillary balance occurs. For real fluids, the viscous phase can be followed by either an intermediate elastic phase or by transition directly to the fully stretched FENE phase depending on the magnitude of the finite chain extensibility b. We conclude by comparing the finite breakup times predicted from the numerical and composite analytic results as the molecular extensibility of the chains varies, and show how these predictions compare with those from Entov and Hinch [11] when the extensibility parameter b becomes very large.

2 Definitions and derivations

In what follows, we consider a cylindrical filament of initial radius R_0, consisting of a dilute polymer solution with solvent viscosity η_s, surface tension σ, at temperature T, containing polymer chains of number density n and molecular weight M_W. The polymer chains are modelled as finitely extensible dumbbells with spring constant H, and fully stretched chain length Q_0. The finite extensibility parameter, related to the ratio between the fully stretched length and equilibrium coil size, is defined as $b = \frac{3Q_0^2}{\langle Q^2 \rangle_{eq}} = \frac{HQ_0^2}{kT}$, where k is the Boltzmann constant and $\langle Q^2 \rangle_{eq}$ is the equilibrium mean square size of the chain. The characteristic relaxation time of the dumbbell is defined as $\lambda_H = \frac{\zeta}{4H}$, where ζ is the Langevin friction coefficient of the beads [18].

In real solutions, the finite extensibility parameter and the relaxation time are related to the molecular weight and the solvent quality through scalings of the form $b \sim M_W^{1-\nu}$, and $\lambda_H \sim M_W^{3\nu}$ respectively, where ν, the excluded volume coefficient characterizing the quality of the solvent, is in the range $0.5 \leq \nu \leq 0.6$ [16]. However, for what follows in this work, in keeping with the approach of Entov and Hinch [11], we treat the relaxation time λ_H and the finite extensibility parameter b as independent variables. Later work will focus on reconciling these parameters with changes in actual molecular structure of the polymer chains, e.g. due to oxidative or mechanical degradation.

2.1 Derivation of the Bird form of the FENE-P constitutive equation

We begin with the constitutive relation for the polymer stress tensor in a dilute suspension of FENE-P dumbbells as derived in [19]:

$$Z\boldsymbol{\tau}_p + \lambda_H \boldsymbol{\tau}_{p_{(1)}} - \lambda_H \left[\boldsymbol{\tau}_p - nkT\boldsymbol{\delta}\right] \frac{D \ln Z}{Dt} = -nKT\lambda_H \dot{\boldsymbol{\gamma}}, \tag{1}$$

where $\boldsymbol{\tau}_p$ is the polymer stress tensor, Z is the FENE term defined as

$$Z = 1 + \frac{3}{b}\left(1 - \frac{tr(\boldsymbol{\tau}_p)}{3nkT}\right), \tag{2}$$

$\dot{\boldsymbol{\gamma}}$ is the symmetric rate of strain tensor and $\boldsymbol{\delta}$ is the unit tensor. This is the form considered by Bird et al [20] which we later use to derive our analytic result.

The dynamics of the problem as well as the governing force balance are specified by assuming a time-varying and axisymmetric uniaxial elongational flow ($v_r = -\frac{1}{2}\dot{\epsilon}(t)r, v_z = \dot{\epsilon}(t)z$) in a cylindrical filament of radius $R(t)$, from which it follows that the time-varying strain rate is given by

$$\dot{\epsilon}(t) = -\frac{2}{R}\frac{dR}{dt}. \tag{3}$$

Combining the force balances in the radial and axial directions, we can eliminate the unknown pressure inside the thinning filament and obtain the following force balance in which the capillary stress is balanced by a combination of the viscous extensional stress difference and the polymer stress difference:

$$\frac{\sigma}{R} = 3\eta_s\dot{\epsilon} - (\tau_{zz} - \tau_{rr}). \tag{4}$$

Eqs. (1)-(4) yield a closed set of equations which can be solved simultaneously in order to obtain the time evolution of the various experimentally observable variables of the problem such as the mid-filament radius $R(t)$.

2.2 Derivation of the Entov and Hinch form of the FENE-P constitutive equation

Additional physical insight can be gained if we express these equations in terms of the microstructural deformation tensor $\mathbf{A}$, as is done by Entov and Hinch [11], instead of the polymer stress tensor $\boldsymbol{\tau}_p$, . The dimensionless tensor $\mathbf{A}$ is related to the ensemble average of the second moment tensor, $\langle\mathbf{QQ}\rangle$ through

$\mathbf{A} = \frac{\langle \mathbf{QQ} \rangle}{\frac{Q_{eq}^2}{3}}$, where $\mathbf{Q}$ is the connector vector (of magnitude Q) between the two ends of the dumbbell, and $\langle . \rangle$ indicates an ensemble average over all dumbbells. As previously stated, the equilibrium coil size is related to the fully stretched coil length through $Q_{eq}^2 = \frac{3Q_0^2}{b+3}$ [16]. The polymer stress is related to the microstructural deformation through the expression $\boldsymbol{\tau}_p = -nkT(Z\boldsymbol{A} - \boldsymbol{\delta})$, where using this notation, the FENE term Z can be expressed as

$$Z = f(tr(\boldsymbol{A})) = \frac{1}{1 - \frac{tr(\boldsymbol{A})}{b}}.$$

Note that since b is generally quite large, we will make the approximation for all that follows that $(b+3) \approx b$. Finally, in order to simplify the calculations to follow, we introduce the parameters $B = \frac{3}{b}$, and $G = nkT$.

By re-expressing the constitutive relation derived in the previous section using this notation, we obtain two ordinary differential equations for the radial and axial microstructural deformations

$$\dot{A_{zz}} = 2\dot{\epsilon}A_{zz} - \frac{1}{\lambda_H}(ZA_{zz} - 1) \tag{5}$$

$$\dot{A_{rr}} = -\dot{\epsilon}A_{rr} - \frac{1}{\lambda_H}(ZA_{rr} - 1). \tag{6}$$

In order to form a closed set of equations, we once again combine these evolution equations for the dumbbell stretch with the kinematic expression for the strain rate $\dot{\epsilon}$ given in Eq.(3) and the force balance from Eq.(4) expressed in terms of the microstructural deformation tensor:

$$\frac{\sigma}{R} = 3\eta_s\dot{\epsilon} + nkTZ(A_{zz} - A_{rr}). \tag{7}$$

In the numerical sections of the work to follow, the coupled system of equations (Eqs. (5)-(7) in combination with Eq. (3)) is solved using the Matlab integration routine ode15s with real and absolute tolerances of 10^{-4} in order to obtain convergent numerical integrations of the complete equation set. The solution of the full system of equations is treated as a reference or 'exact' solution. However, we show in the following section that with a couple of additional simplifications, an analytic solution for the capillary thinning of a solution of FENE dumbbells can also be obtained.

3 Analytic solution

Numerical simulations suggest that after an initial phase in which the solvent viscosity is important (and which we consider in detail later in Section 5), the capillary pressure becomes nearly entirely balanced by the axial contribution to the polymer stress in the thinning and elongating filament. In this regime, it is justified to make two additional assumptions in order to simplify the problem further: firstly, that the radial and tangential contributions to the stress tensor are negligible; and secondly that the viscous extensional stress difference is negligible.

From Eq. (4), the approximate force balance becomes

$$\tau_{zz} \approx -\frac{\sigma}{R}. \tag{8}$$

Substituting this result, as well as that for the strain rate $\dot{\epsilon}(t)$ given in Eq. (3) into the constitutive equation given in Eq. (1) yields an ordinary differential equation for the midpoint radius R in terms of time t only.

$$\frac{\mathrm{d}R}{\mathrm{d}t}\left(-\frac{3\sigma}{R}+\left(\frac{\sigma}{R}+G\right)\frac{B\sigma}{3GR(B+1)+B\sigma}+\frac{4G}{\sigma}\right)=-\frac{1}{\lambda_H}\left(1+B\left(1+\frac{\sigma}{3GR}\right)\right) \tag{9}$$

At this point, it is useful to define some non-dimensional numbers in order to further simplify the equations to follow. We introduce a non-dimensional radius, $\xi = \frac{R}{R_0}$, a non-dimensional time, $\tau = \frac{t}{\lambda_H}$, and an elastocapillary number, $E_c = \frac{GR_0}{\sigma}$, which is the ratio between the elastic modulus $G = nkT$ of the dilute suspension of dumbbells and the initial capillary pressure $\frac{\sigma}{R_0}$. Following [11], we also introduce a final non-dimensional parameter to scale the relative magnitude of the solvent viscosity, $S = \frac{\eta_s}{G\lambda_H} = \frac{\eta_s}{\eta_p}$, which we discuss in detail further below. Typical ranges of these parameters for biological fluids are $\eta_s \sim 1 - 100\ mPa\ s$, $\lambda_H \sim 1 - 1000\ ms$, $E_c \sim 0.001 - 1$ [21], and $S \geq 1$.

Eq. (9) can be solved analytically, and using the initial condition that at non-dimensional time $\tau = 0$ the non-dimensional radius is $\xi = 1$, we obtain an implicit solution for the evolution of the radius with time, given by

$$\left(\frac{1}{1+E_c(b+3)}-\frac{1}{1+\xi E_c(b+3)}\right)+3\ln\left(\frac{1+\xi E_c(b+3)}{1+E_c(b+3)}\right)+4E_c\frac{(b+3)}{(b+2)}(\xi-1)=-\frac{(b+3)^2}{b(b+2)}\tau. \quad (10)$$

In Figure 1, we plot the evolution of the nondimensional radius against the nondimensional time for various values of the finite extensibility parameter, b. In keeping with the choice of Entov and Hinch, the elastocapillary number is taken to be $E_c = 0.001$ [11]. The effect of increasing b is clearly to slow down the thinning of the filament and delay the time to breakup. When b is small, the polymer chains reach their fully stretched length relatively early in the thinning process. At this point, the viscosity of the FENE fluid essentially becomes constant at a high value corresponding to the steady state extensional viscosity, and the radius decays linearly in time. However, when b becomes sufficiently large, the chains continue to be able to stretch elastically and resist the increasing capillary pressure for progressively longer filament thinning times before reaching their finite extensibility limit. In the limit of $b \to \infty$, finite extensibility effects are never felt, and the Oldroyd-B solution corresponding to an exponential decrease in the radius is recovered. This limit will be explored in detail in the next section.

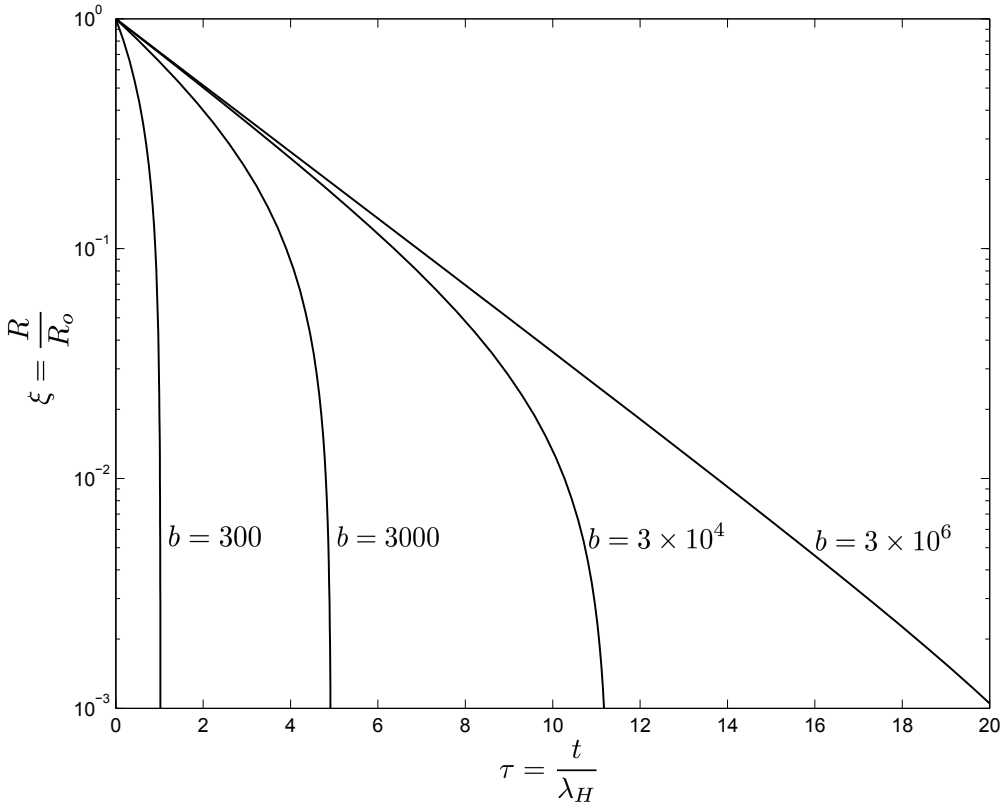

Figure 1: Evolution of the non-dimensional radius ξ versus non-dimensional time τ for various values of the finite extensibility parameter b with an elastocapillary number $E_c = 0.001$ and $S = 0$.

Perhaps the most useful outcome of this solution is the ability to obtain an exact analytic result for the finite time to breakup of the filament, t_{break}. By substituting $\xi = 0$ into Eq. (10), we obtain the following expression

$$\frac{t_{break}}{\lambda_H} = \tau_{break} = \frac{b(b+2)}{(b+3)^2}\left(\frac{E_c(b+3)}{1+E_c(b+3)} + 3\ln(1+E_c(b+3)) + 4E_c\frac{(b+3)}{(b+2)}\right). \tag{11}$$

This result allows us to quantify an important experimentally observable property for a thinning thread of a complex fluid, the finite time to breakup, using only two non-dimensional microstructural parameters; the molecular extensibility b of the chain and the elastocapillary number E_c. As $b \to \infty$, the breakup time diverges because the chains can stretch indefinitely. This limit of infinite extensibility is considered in the next section.

4 Limit of infinite extensibility ($b \to \infty$)

In the limit of infinite extensibility of the chains, $b \to \infty$ (or $B = 0$), Eq. (10) for the evolution of the non-dimensional radius ξ reduces to

$$3\ln(\xi) + 4E_c(\xi - 1) = -\tau. \tag{12}$$

At early times, when the mid-filament radius is still close to R_0, ξ can be written as $\xi = 1 - \delta$, where $\delta << 1$. Substituting this expression into Eq. (12) and expanding the logarithmic term, we see that the radius initially evolves linearly in time as

$$\xi \approx 1 - \frac{\tau}{3 + 4E_c}. \tag{13}$$

At later times, as $\xi \to 0$, the logarithmic term dominates and Eq. (12) predicts that the radius decays exponentially as

$$\xi = e^{4E_c/3} e^{-\tau/3}. \tag{14}$$

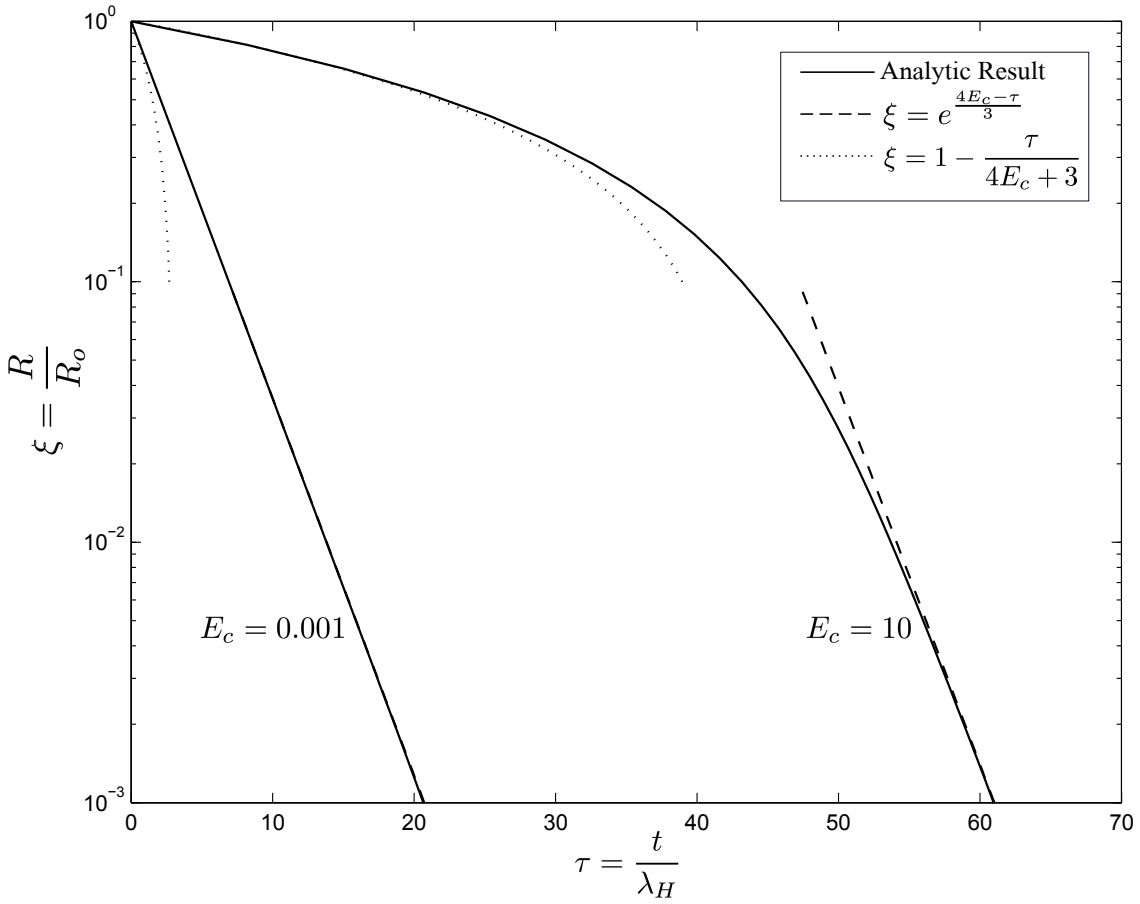

Figure 2: Effect of the elastocapillary number E_c on the evolution of the non-dimensional radius ξ as a function of the non-dimensional time τ, for the infinite extensibility limit of $b \to \infty$. The linear limit given in Eq. (13) is shown by the dotted line, and the later exponential limit in Eq. (14) is shown by the dashed line.

Entov and Hinch also present an analytic result for the radius evolution derived from Eqs. (5)-(7) during what they term the "middle elastic time"; the period following the viscous dominated regime, when viscous contributions to the extensional stress can be ignored and finite extensibility effects are negligible. It is evident from Figure 1 that when b is small, this period is not necessarily encountered, as finite extensibility effects become important essentially as soon as polymer stresses become significant enough to play a role in the force balance. This is an important consideration when attempting to extract viscoelastic properties from CaBER experiments for dilute polymer solutions, as the relaxation time can only be obtained from radius evolution data if the exponential decay regime characteristic of elastocapillary thinning is encountered [22, 23, 24]. A criterion for achieving this exponential elastocapillary balance based on a minimum polymer concentration and molecular weight (or extensibility) argument has been discussed by Campo-Deaño and Clasen [22]. Recently, however, Sachsenheimer et al have shown that good measurements of the extensional relaxation time can still be obtained from filament sagging measurements and force calculations using a tilted CABER, even if this exponential thinning regime is not established [23]. We examine the detailed dynamics of this transition to polymer stress dominated thinning later in this work.

The appropriate analogous period to Entov and Hinch's [11] "middle elastic time" in the present analytic solution corresponds to late times when $b \to \infty$, for which the solution to the capillary thinning equation is given in Eq. (14). Following the arguments of Entov and Hinch [11], analysis of Eq. (2) indicates that when finite extensibility effects are negligible, we can take $Z \approx 1$. Substituting this approximation and Eq. (3) along with the assumption that $A_{zz} - 1 \approx A_{zz}$ into Eq. (5), we obtain the following evolution equation

$$\frac{dA_{zz}}{dt} = -A_{zz}\left(\frac{4}{R}\frac{dR}{dt} + \frac{1}{\lambda_H}\right), \tag{15}$$

which, using the initial condition ($R = R_0$ and $t = t_0$), as previously done, yields

$$A_{zz} = \left(\frac{1}{\xi}\right)^4 e^{-\tau}. \tag{16}$$

Under these conditions and the assumption that the radial and tangential contributions to the polymer stress are again negligible, the force balance in Eq. (7) reduces to an elastocapillary balance of the form

$$\frac{\sigma}{R} = GA_{zz}. \tag{17}$$

Finally, combining Eqs. (16) and (17) yields Entov and Hinch's expression [11] for the non-dimensional radius evolution during the middle elastic time:

$$\xi^{(EH)} = E_c^{1/3} e^{-\tau/3} = \left(\frac{nkTR_0}{\sigma}\right)^{1/3} \exp\left(-t/3\lambda_H\right). \tag{18}$$

This result is clearly inconsistent with what was obtained analytically in Eq. (14). For a typical value of the elastocapillary number $E_c = 0.001$ at time $\tau = 0$, Eq. (18) predicts that $\xi = E_c^{1/3} = 0.1$, while Eq. (14) predicts that $\xi = e^{4E_c/3} \approx 1$. It is clear then that the assumption made in deriving our analytic solution in Eq. (10) that the solvent viscosity could be neglected entirely is not true in this parameter range. Indeed, for dilute polymer solutions, there is an initial period of filament thinning during which the viscous extensional stress dominates over the polymer stress contribution. Results derived from the full numerical solution accurately capture this initial period (see for example Clasen at al [16]), which explains why, unlike the analytic result, simulations show that when the middle elastic time begins, the corresponding value of the radius is $R < R_0$.

This analysis motivates the need for a composite analytic result, in which the analytic solution derived above for the radius evolution during the polymer stress-dominated capillary thinning regime is combined with an appropriate short time solution in the early viscous regime. Determining how to construct this composite analytic result and comparing it with direct numerical solution of Eqs. (5)-(7) will be the focus of the remainder of this manuscript.

5 Composite analytic result

In order to formulate the composite analytic solution, two remaining items are needed: first, we must solve for the temporal evolution of the radius during the initial viscous regime, and second, we must determine the point at which the transition to the polymer stress dominated regime occurs.

At this time, we more formally introduce the final non-dimensional parameter, $S = \frac{\eta_s}{\eta_p} = \frac{\eta_s}{G\lambda_H}$, which gives the ratio between the solvent and polymer contributions to the viscosity, where the latter is given

by $\eta_p = G\lambda_H$. We can also express this ratio in terms of polymer concentration by writing the zero-shear viscosity in expanded form as $\eta_0 = \eta_s(1 + c[\eta] + ...) = \eta_s + \eta_p$, where c is the concentration of polymer chains and $[\eta]$ is the intrinsic viscosity. It follows that $S = \frac{1}{c[\eta]}$. Since the coil overlap concentration c^* scales as $c^* \sim \frac{1}{[\eta]}$, then $S \approx \frac{c^*}{c}$ [16]. From this result, it is clear that in order for the polymer solution to be dilute, which is the case for many biological fluids, we require that $S \geq 1$, and for the remaining figures, we generally use $S = 1$ to be consistent with Entov and Hinch [11]. The solution given in Eqs.(10),(11) is relevant only in the limit $S << 1$.

5.1 Early viscous regime

Addressing the first item noted above, if $S \geq 1$, then early in the thinning process (before the polymer chains have been sufficiently stretched to begin contributing to resisting the capillary pressure that drives the thinning filament) the force balance in Eq. (4) simplifies to

$$\frac{\sigma}{R} = 3\eta_s\dot{\epsilon}. \tag{19}$$

Before continuing on to the solution of this equation during the early viscous regime, however, a more in-depth consideration of the viscocapillary balance in Eq.(19) is merited.

Up until this point, all derivations have assumed a perfectly cylindrical filament at all times during the thinning process. Although this is a reasonably good approximation late in the thinning process when polymer stresses are dominant (which is the case that the analytic solution considers), there is ample evidence that early on during the initial viscous thinning phase, the curvature of the filament is quite important [25, 26] (though this will not affect the agreement between the analytic model and numerical simulations since both assume a cylindrical filament). We therefore introduce the notation of Tripathi and McKinley [25], derived for viscous Newtonian fluids, to account for the axial filament curvature and enable quantitative agreement between the composite analytic solution and experimental data.

By assuming a perfectly cylindrical thread of Newtonian fluid attached to infinite reservoirs at either end, the solution assumes that the net longitudinal stress in the solvent is 0 for all times. In this limit, the axial tension in the filament arising from surface tension is

$$F_z(t) = 2\pi\sigma R_{mid}(t).$$

Tripathi and McKinley show that in fact the axial curvature and the resulting viscous longitudinal stress in the filament is non-zero, and good agreement can be achieved with experimental data by incorporating a correction factor $X(t)$ such that $F_z(t) = X(t) \times 2\pi\sigma R_{mid}(t)$. Numerical solution of the similarity solution presented by Papageorgiou for slender viscous threads shows that the value of $X(t)$ converges to a constant given by $X(t) \approx 0.7127$ [27]. As such, the modified force balance during the initial viscous thinning period is found to be

$$(2X-1)\frac{\sigma}{R} = 3\eta_s\dot{\epsilon}, \tag{20}$$

where it is simple to see that $X = 1$ recovers the initial cylindrical filament solution [25].

Substituting the expression given in Eq. (3) for $\dot{\epsilon}$ into Eq. (20) and integrating using the initial condition $R = R_0$ at $t = 0$, we find the well known result that during the initial viscous regime, the filament radius decays in a linear fashion given by

$$\xi = 1 - \frac{(2X-1)\tau}{6SE_c}. \tag{21}$$

From this relationship, we can derive the viscous breakup time t_c at which a Newtonian filament (in which the only term opposing the capillary pressure is the viscous extensional stress difference) would break. To find t_c, we set $\xi = 0$ in Eq. (21), and obtain

$$t_c = \frac{6SE_c\lambda_H}{(2X-1)} = \frac{6\eta_s R_0}{\sigma(2X-1)}. \tag{22}$$

From Eq. (3), it follows that the strain rate during the viscous regime is given by

$$\dot{\epsilon} = \frac{2}{\lambda_H(\tau_c - \tau)}, \tag{23}$$

where $\tau_c = {}^{t_c}/_{\lambda_H} = \frac{6SE_c}{(2X-1)}$.

Since elastic stretching of the chains starts from equilibrium conditions, during this period finite extensibility effects are negligible, and so again we take $Z = 1$. From Eq. (5) and the relationship for $\dot{\epsilon}$ during the linear viscocapillary period (Eq. (23)), we find that the early axial microstructural deformation is given by

$$A_{zz} = \left(\frac{\tau_c}{\tau_c - \tau} \right)^4 e^{-\tau}. \tag{24}$$

Figure 3 shows the evolution of the axial microstructural deformation A_{zz} at very early times for various values of the finite extensibility parameter b. The solution obtained for A_{zz} during the initial linear viscous period is shown by the dashed blue line. It can be seen that this expression diverges at the viscous breakup time, τ_c, as derived in Eq. (22) and shown in Figure 3 by the broken (black) line. However, for short times $\tau < \tau_c$, Eq.(24) provides a very good analytic expression for the evolution in $A_{zz}(t)$ for all values of b (large or small).

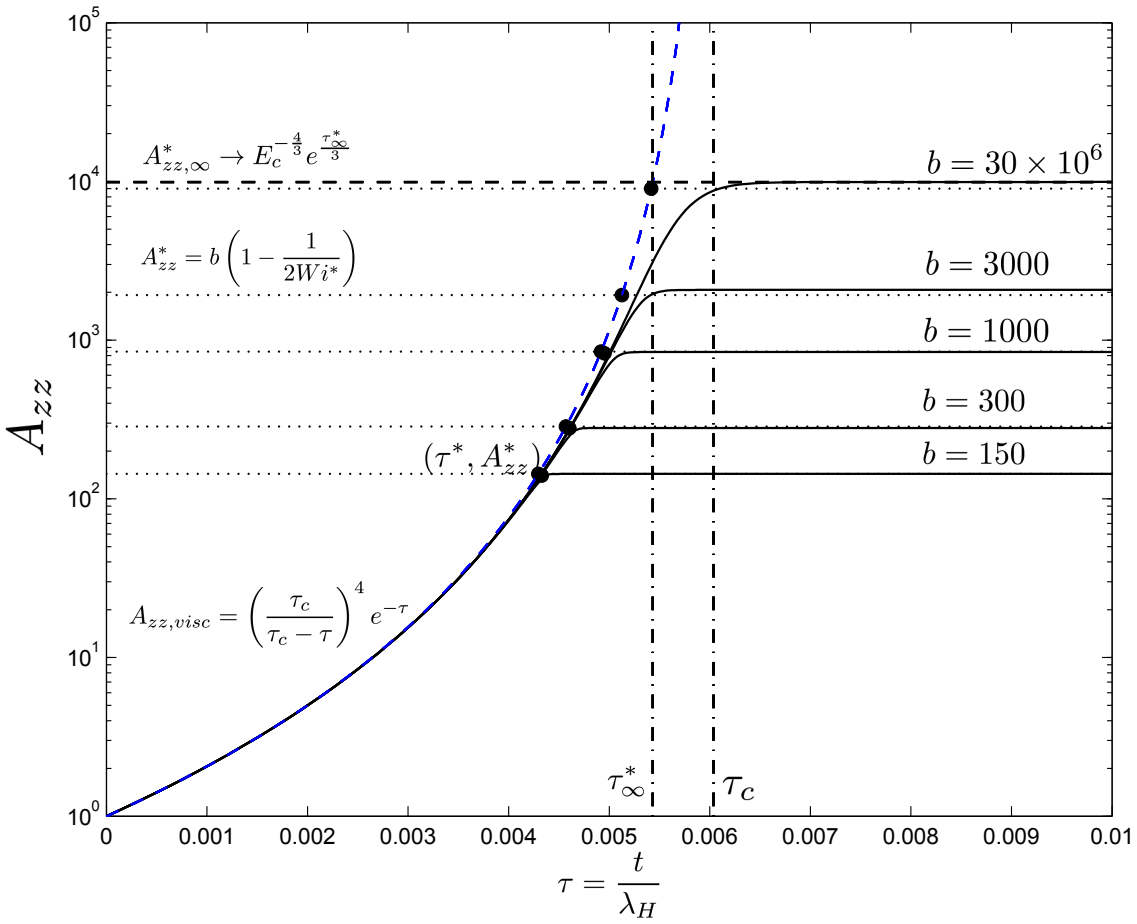

Figure 3: Effect of varying the finite extensibility parameter b on the level of axial microstructural deformation A_{zz} near the transition point at which the viscous regime ends. The solid black lines correspond to the numerical simulations, and the dashed blue line denotes the evolution of A_{zz} during the viscous regime as given in Eq. (24). The solid dots denote the transition points (τ^*, A_{zz}^*) that need to be determined for the composite analytic solution. The breakup time for a Newtonian fluid, τ_c, and the transition time τ_∞^* in the limit of infinite extensibility, are shown with dot-dashed lines. As b is reduced, the level of axial microstructural deformation departs from the viscocapillary solution increasingly early as a result of the limited extensibility of the constituent dumbbells and plateaus at $A_{zz}^* = b\left(1 - \frac{1}{2Wi^*}\right) \approx b$ as given in Eq. (27). As b becomes very large, τ^* approaches the infinite extensibility transition time τ_∞^*, and the plateau value of A_{zz} approaches that predicted during the "middle elastic time", $A_{zz,\infty}^*$, given in Eq. (16) and shown by the dashed black line.

5.2 Transition to the polymer stress dominated regime

Now to address the second remaining issue, we note from Figure 3 that at some time t^* and radius R^* and corresponding value of the polymer stretch A_{zz}^* (where the star superscript denotes the transition point value of each variable) the extensional stress resulting from the stretching of the polymer chains becomes comparable in magnitude to the viscous contribution from the solvent. We determine this transition time by considering the point at which both the viscocapillary and elastocapillary balances

hold simultaneously. The former arises from the early linear viscocapillary regime and is given by

$$\frac{\sigma}{R^*} = \frac{3\eta_s \dot{\epsilon_v}^*}{(2X-1)} \tag{25}$$

where $\dot{\epsilon_v}^*$ is the strain rate at time t^*, as determined from Eq. (23), $\dot{\epsilon}_v^* = \frac{2}{\lambda_H(\tau_c - \tau*)}$. Simultaneously, a new force balance (as given in Eq.(7) with only the axial stress term retained) develops between the capillary pressure and the combined resistance of the viscous and the polymer contributions to the tensile stress. In order to be able to satisfy this new relationship for the same value of the capillary stress, the strain rate must instantly drop to some new lower value, $\dot{\epsilon}^* < \dot{\epsilon_v}^*$, and equating this force balance with the viscous one from Eq.(25) yields the relationship

$$\frac{3\eta_s \dot{\epsilon_v}^*}{(2X-1)} = \frac{\sigma}{R^*} = 3\eta_s \dot{\epsilon}^* + nkTZ^* A_{zz}^*. \tag{26}$$

It remains to determine the transition point values of the axial microstructural deformation A_{zz}^*, axial polymer stress $\tau_{zz}^* = -nkTZ^*A_{zz}^*$, and finite extensibility parameter Z^*. At the transition point (t^*, R^*), the numerical simulations shown in Figure 3 as the solid black lines indicate that the axial microstructural deformation reaches an approximate plateau value. The maximum deformation the polymer chains can reach is limited by the finite extensibility parameter, b. When b is small, the chains are nearly fully extended once this plateau occurs and $A_{zz}^* \approx b$. Clearly, FENE effects are non-negligible in this regime, and so the force balance derived during the "middle elastic time" is not valid. As b increases, the chains continue to extend after the linear viscous regime ends, but it is evident from Figure 3 that the time rate of change of A_{zz} is comparatively very small (in dimesionless terms because of the large elastic stress difference that arises for finitely extensible chains). Therefore, at the transition point, we make the approximation that $\dot{A_{zz}} \approx 0$, which from Eq. (5) yields that $Z^* \approx 2Wi^*$, where Wi^* is the Weissenberg number at this transition, defined as $Wi^* = \lambda_H \dot{\epsilon}^*$. From the definition of Z (Eq. (2)) we obtain

$$A_{zz}^* = b\left(1 - \frac{1}{2Wi^*}\right). \tag{27}$$

By substituting the expression for A_{zz}^* given in Eq.(27) and the expression for $\dot{\epsilon_v}^*$ derived above into Eq.(26) we obtain the final result for the crossover force balance

$$3\eta_s \frac{2}{\lambda_H(\tau_c - \tau*)(2X-1)} \simeq \frac{\sigma}{R^*} \simeq 3\eta_s \dot{\epsilon}^* + 2G\lambda_H b\dot{\epsilon}^* \left(1 - \frac{1}{2Wi^*}\right). \tag{28}$$

Both the solvent contribution and the FENE contribution from the extended polymer chains are therefore viscous in character (i.e. they scale linearly with $\dot{\epsilon}^*$). For all that follows, we take $X = 1$ for simplicity, and drop the factor of $(2X - 1)$ from the initial viscous solution, although retention of this factor or substitution of $X = 0.7127$ from the Papageorgiou similarity solution would neither be difficult nor would it alter the nature of the analysis to follow. Solving Eq.(28) yields a first relationship between the rate of strain at the crossover $\dot{\epsilon}^*$ and the crossover time τ^*

$$\dot{\epsilon}^* = \frac{\frac{2}{\lambda_H(\tau_c - \tau^*)} + \frac{Gb}{3\eta_s}}{1 + \frac{2Gb\lambda_H}{3\eta_s}}. \tag{29}$$

The second relationship is found from the fact that at the transition point, the axial microstructural deformation is constant in both regimes on either side of the 'pinch'. In other words, because $\dot{A_{zz}} \approx 0$ we have at t^* that

$$\left(\frac{\tau_c}{\tau_c - \tau^*}\right)^4 e^{-\tau^*} = A^*_{zz} = b\left(1 - \frac{1}{2Wi^*}\right). \tag{30}$$

This yields a second equation for $\dot{\epsilon}^*$ in terms of τ^*,

$$\dot{\epsilon}^* = \frac{1}{2\lambda_H}\left[1 - \frac{e^{-\tau^*}}{b}\left(\frac{\tau_c}{\tau_c - \tau^*}\right)^4\right]^{-1}. \tag{31}$$

Finally, we solve for the crossover or transition time τ^* by equating Eqs. (29) and (31) to obtain, in non-dimensional form, the following implicit expression for τ^*:

$$\frac{1}{2}\left(1 - \frac{e^{-\tau^*}}{b}\left(\frac{\tau_c}{\tau_c - \tau^*}\right)^4\right)^{-1} = Wi^* = \frac{\frac{2}{\tau_c - \tau^*} + \frac{b}{3S}}{1 + \frac{2b}{3S}}. \tag{32}$$

From this expression, τ^* can be solved for numerically, and the result is then used to compute the modified strain rate $\dot{\epsilon}^*$ and the plateau value of the various other parameters such as Z^* and Wi^*. The dimensionless radius at the transition point, ξ^*, is found from substituting this result for τ^* into Eq. (21).

It is important to note that when b approaches the limit of infinite extensibility ($b \to \infty$), FENE effects and the viscous contribution to the total extensional stress are indeed negligible during this elastocapillary period, and at the end of the viscous regime the solution does transition to the "middle elastic time" defined by Entov and Hinch [11] and in Section 2.2. In Eq. (18), we derived an explicit result for the rate of radius evolution in this regime. We can therefore combine this result with the linear evolution of

the filament radius (Eq. (21) here with $X = 1$) expected in the initial viscocapillary regime in order to determine the transition time $\tau^*_\infty = {}^{t^*_\infty}/_{\lambda_H}$ in the limit of infinite extensibility

$$1 - \frac{\tau^*_\infty}{6SE_c} = E_c^{1/3} e^{-\tau^*_\infty/3}. \tag{33}$$

The value of the filament radius at the transition point (denoted R^*_∞), follows from either equation ((18) or (21)). Since the "middle elastic time" is simply a special case of the early FENE period with $Z = 1$ and $\dot{\epsilon}^*$ sufficiently small that the viscous extensional stress is negligible, as $b \to \infty$ the two transition points converge with

$$\lim_{b\to\infty} (t^*, R^*) \to (t^*_\infty, R^*_\infty). \tag{34}$$

The plateau value for the microstructural deformation in the limit of $b \to \infty$ can also be derived by combining Eqs. (16) and (18), which are both valid during the "middle elastic time", to obtain

$$A^*_{zz,\infty} \to E_c^{-4/3} e^{\tau^*_\infty/3}. \tag{35}$$

Although in general we must solve for this crossover time τ^* given in Eq.(32) numerically, in certain limits an analytic expression can be obtained. If we consider S to be of order unity, then the non-dimensional transition time τ^* is very small (typically on the order of 10^{-3}) and the exponential term in Eq. (32) can be approximated as unity. In the limit of large finite extensibility parameter b, a Taylor expansion of Eq.(32) then gives

$$\tau^* \approx \tau_c (1 - E_c^{1/3}) \tag{36}$$

It is simple to see that this analytic result for the case of $b \to \infty$ is in agreement with the solution obtained for the "middle elastic time" (Eq. (33)) for the limit of $\tau^*_\infty = {}^{t^*_\infty}/_{3\lambda_H} \to 0$.

Finally, we summarize the steps required in order to construct the composite analytic solution, and then plot and compare this result with the numerical solution. We first obtain the transition time for crossover from a viscocapillary to elastocapillary balance τ^* by solving Eq. (32) numerically, where for $\tau < \tau^*$, the radius evolution is given by the linear viscous result from Eq. (21). For times $\tau > \tau^*$, the mid-filament radius evolution $\xi(\tau)$ is given by the analytic result in Eq. (10), although the initial radius is no longer

R_0 since there has already been capillary thinning during the initial linear viscocapillary regime. We account for this by defining a new effective elastocapillary number E_c^*, which reflects the fact that the elastocapillary thinning period actually begins with a smaller effective initial mid-filament radius, R_0^* than the initial plate radius. We obtain this new radius by numerically solving Eq. (10) for the value of R_0^*. We can then calculate the effective elastocapillary number through the rescaling $E_c^* = E_c \frac{R_0^*}{R_0}$. Finally, with this effective elastocapillary number, we can obtain an exact analytic expression for the finite time to breakup of the filament (which has taken account of the initial importance of the viscosity of the solvent at early times using Eq. (11)).

In Figure 4, we plot the evolution of the non-dimensional radius ξ as a function of the non-dimensional time τ for the numerical, analytic, and composite analytic solutions with $E_c = 0.01$ and a reasonably large value of the finite extensibility parameter, $b = 3 \times 10^4$, for three different values of the non-dimensional solvent viscosity, S. The analytic elastocapillary solution from Eq. (10), shown by the dashed-dotted black line, clearly overpredicts the full numerical result on account of its neglect of the initial period of rapid viscocapillary thinning. The inset shows how the composite analytic solution is created, as summarized above. We begin with the linear viscocapillary balance (from Eq. (21)), shown by the dotted line for each value of S, which matches the corresponding numerical result very well at early times $\tau < \tau^*$. At the transition point, denoted (τ^*, ξ^*), (and shown by a large star in the inset figure), we reinitialize our analytic elastocapillary result, defined with a new effective radius R_0^* (or equivalently a new elastocapillary number E_c^*), and depicted by a solid line. The reinitialized form of Eq.(11) then can be used to find τ_{break}. Especially for small and moderate values of S, the composite analytic result matches the numerical solution nearly exactly for the entire thinning process, as can be seen in the main graph.

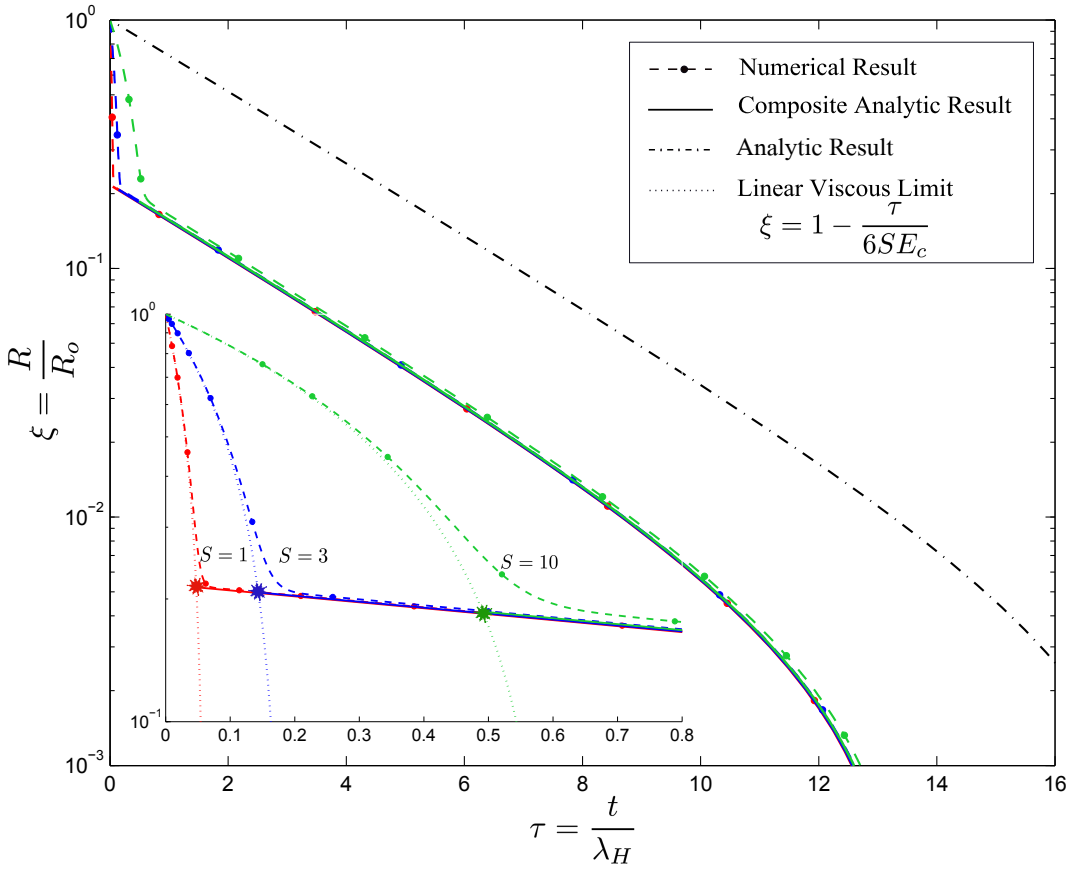

Figure 4: Comparison of the numerical, analytic, and composite analytic results for the evolution of the non-dimensional radius ξ as a function of the non-dimensional time τ for $E_c = 0.01$, $b = 3 \times 10^4$, and three different values of the non-dimensional viscosity $S = {}^{\eta_s}/_{\eta_p}$. The red curve denotes $S = 1$, the blue curve denotes $S = 3$, and the green curve denotes $S = 10$. The composite analytic result, composed of the linear viscous result and the analytic result from Eq. (10) adjusted for the new effective initial radius R_0^*, matches the full numerical solution very well. The analytic result from Eq. (10) overpredicts the radius due to its neglect of the solvent viscosity which dominates the initial rapid stretching phase. The inset shows that the solvent viscosity ratio S affects the solution only at very early times. The principal effect being to delay the transition point (τ^*, ξ^*), denoted by a star, as a result of the polymer stresses being comparatively smaller for longer times. However, once elastic stresses dominate, the value of S becomes irrelevant.

Clearly, the effect of increasing the non-dimensional solvent viscosity ratio S is to delay the transition time at which the thinning becomes dominated by elastic polymer stresses as opposed to viscous extensional ones. We note that S is increased by increasing the solvent viscosity η_s, and that a delay in the transition time is associated with a decreased value in the filament radius R^* at which the transition ultimately occurs. This can clearly be seen in the inset of Figure 4. As the solvent viscosity is increased from $S = 1 \rightarrow 10$, the viscous extensional stress grows correspondingly as well, and so the polymer chains must be stretched more and more before the polymer stresses become significant components of the total force balance. It follows that the finite time to breakup also increases with S (for fixed values of λ_H

and b), although for the parameter range chosen in Figure 5 the overall effect is rather small. From Eq. (18), it is clear that the effect of increasing the elastocapillary number E_c, either by increasing the initial radius R_0, the temperature T, or chain density n, or decreasing the surface tension of the solution σ, is to increase the radius at the transition point R^*, which implies an earlier transition to the elastocapillary thinning regime. As a result, the effect is also to increase the time to breakup of the filament, since more of the thinning process occurs at the relatively lower exponential thinning rate of the elastocapillary regime as opposed to the initial rapid linear thinning rate that results from a viscocapillary balance.

6 Analytic expression for the breakup time

The use of the new effective initial radius for the elastocapillary balance R_0^* and a corresponding effective elastocapillary number E_c^* in order to account for the initial viscous thinning period allows us to solve for the finite time to breakup of the filament analytically using Eq. (11).

In Figure 5, this breakup time is plotted as a function of the finite extensibility parameter b for both our composite analytic result (solid line) and the numerical solution of Eqs. (3) and (5) -(7) (filled points). For the purposes of numerical computation, the breakup time is chosen to correspond to the time at which $\xi^* \to 10^{-4}$. It can be seen that the two results match very well over the whole range of values of b considered.

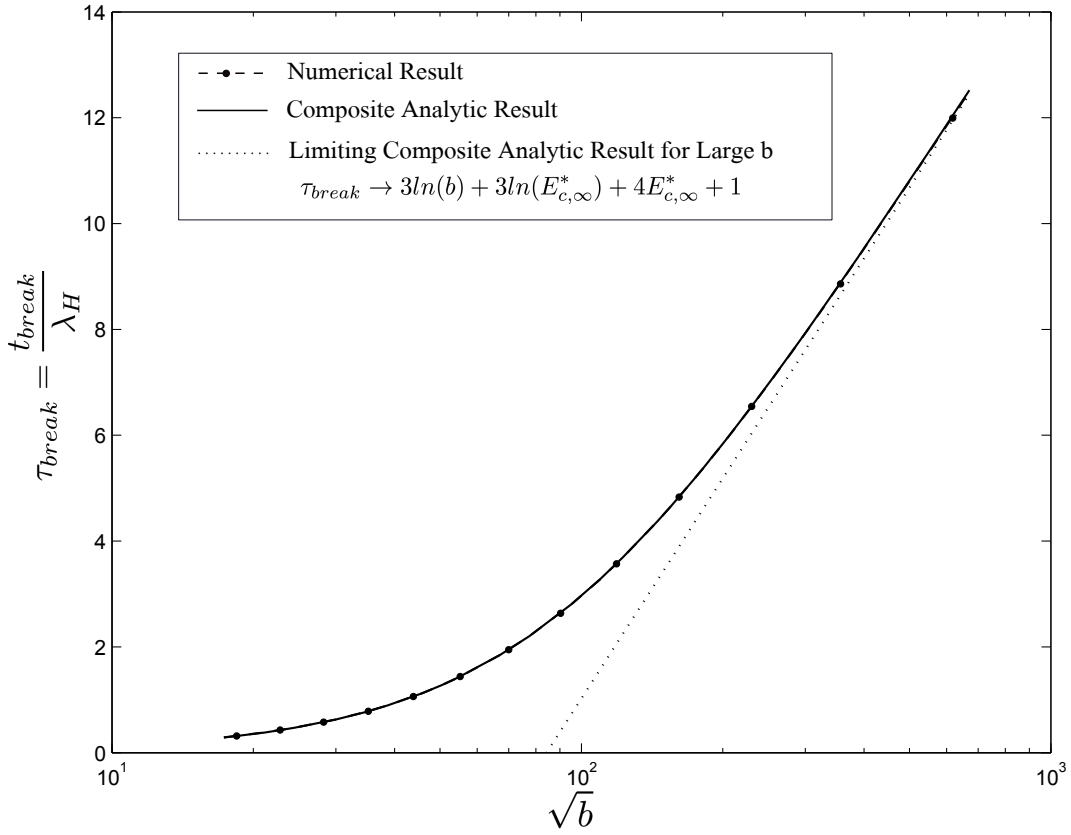

Figure 5: Comparison of the predicted breakup time from the numerical and composite analytic solutions, as a function of the finite extensibility parameter b. The elastocapillary number is taken to be $E_c = 0.001$ and the non-dimensional viscosity is taken to be $S = 1$ in order to provide comparison with the results presented by Entov and Hinch [11]. The two results agree very well, and converge to the limiting analytic result when the finite extensibility parameter approaches infinity.

Entov and Hinch [11] present an analytic result for the breakup time at large b (for a simplified case of their model in which the fluid is assumed to have a single relaxation time) given by

$$\tau_{break}^{(HE)} \rightarrow 3\ln\left(\frac{4b}{3}\right) + 4\ln(E_c) + 3. \tag{37}$$

They state that this equation overpredicts the results that they obtain from their full numerical solution rather significantly [11]. By using the solution for the breakup time given in Eq. (11),it can readily be shown that in the limit of $b \rightarrow \infty$, Eq. (11) becomes

$$\tau_{break} \rightarrow 3\ln(b) + 3\ln(E^*_{c,\infty}) * + 4E^*_{c,\infty} + 1 \tag{38}$$

where $E^*_{c,\infty} = E_c\xi^*_\infty$ is the effective rescaled elastocapillary number in the limit of infinite extensibility that is relevant after crossover to the elastocapillary balance.

This result is plotted as the dotted line in Figure 5. At large values of the finite extensibility parameter corresponding to $\sqrt{b} \gtrsim 300$, both the composite analytic and numerical solutions converge to this asymptotic result that is appropriate for very large (but finite) values of the extensibility parameter. Thus, our result improves on the expression derived by Entov and Hinch [11] (Eq. (37)).

7 Conclusions

In this work we have derived a composite analytic solution that describes the complete time evolution of the filament radius and the finite time to breakup of a FENE-P fluid filament undergoing elastocapillary thinning. The composite analytic solution consists of an initial viscocapillary regime characterized by an initial linear decrease in the filament radius (see Eq. (21)), followed by a rapid crossover (or 'pinch point') to an elastocapillary regime dominated by the polymer stress, for which we have determined an analytic expression for the evolution of the filament radius (see Eq. (10)). The time and radius at which the crossover between the two regimes occurs, denoted (t^*, R^*) respectively, can be approximated analytically by considering simultaneous force balances: during the initial linear regime, it is assumed that the viscous extensional stress alone balances the capillary force; while in the second regime, both the viscous extensional stress and the FENE polymer stress are important. By determining this pinch point and rescaling the initial radius for our analytic elastocapillary balance to be R_0^*, the finite breakup time can be derived and is given by Eq. (11). We have also noted that in the limit of infinite chain extensibility ($b \to \infty$), this transition point converges to values (t_∞^*, R_∞^*), which correspond to an alternate elastocapillary balance in which capillary forces are opposed only by neo-Hookean polymer stresses (without FENE effects) and the viscous extensional stress is negligible. This corresponds to the "middle elastic time" regime first considered by Entov and Hinch [11]. We have also shown that our composite analytic solution matches very well with the full numerical simulations over a wide range of fluid parameters in terms of both the time evolution of the mid-filament radius $R(t)$ and the finite time to breakup. Although negligibly small, these simulations do incorporate the contribution of the radial stresses.

As has been shown before, both numerically (see for instance Entov and Hinch [11]) and experimentally (Anna [14]), our composite analytic solution also predicts that the time to breakup of the filament depends strongly on the molecular weight of the polymer in solution through the finite extensibility pa-

rameter b, where $b \sim M_W^{1-\nu}$. Indeed, from our analytic expression for the breakup time in Eq. (38) in the limit of large extensibility, we show that $\tau_{break} \sim 3\ln(b) \sim 3(1-\nu)\ln M_W$. This result is interesting in the context of using CaBER as a diagnostic tool for probing the rheological state of biological fluids, particularly sensitive materials which begin to degrade once a fluid sample has been collected. A specific example of relevance here is the loss of viscoelasticity of saliva with age once it has been extracted from the mouth. Aggazzotti reported this observation in as early as 1922 [28] in his ground-breaking studies of *potere filante* or filament forming potential. He performed a series of experiments on saliva at various ages, such as stretching filaments until they broke and recording their maximum extensions, and examined the solubility of saliva components through the addition of acetic acid. His results showed a decrease in the maximum extension length of the thread, as well as an increase in the solubility of saliva as it aged. Although he did not draw this conclusion himself, both results suggest that as saliva ages, the molecular weight, and thus the characteristic relaxation time (λ_H) and molecular extensibility (b), of the principal biopolymer contained in saliva (i.e. the MUC5B mucin) decreases as a result of biological decomposition mechanisms. This also appears to be consistent with the findings of Basilevsky and coworkers with regards to bacterial degradation of sputum [7]. It will be of future interest to see whether degradation in the molecular weight of the MUC5B chains can be systematically monitored and modelled using the finite breakup time derived from the FENE-P model presented herein and tested against results from CaBER experiments. Care must be taken when extracting molecular weight values at various stages of degradation from the values of b extracted from filament thinning measurements, as previous work has shown that the FENE-P model can substantially overpredict the true tensile stress in strong transient elongational flows [29, 30]. However, in the quasi-steady FENE limit in which the chains are close to fully stretched, much better agreement with the values expected from molecular theory can be obtained [31].

Finally, we note that part of the challenge in determining the composite analytic solution arises from determining the crossover point (t^*, R^*) between the initial viscocapillary and (finitely extensible) elastocapillary balance that develops at later times. Determining this crossover accurately is important for establishing the characteristic length scale on which elastic effects become important in dilute polymer solutions. However, as the concentration of dissolved polymer increases (and S decreases), or as the network forming character of the fluid sample increases, this term becomes progressively less important. This can be easily observed experimentally by the absence of an initial viscocapillary thinning phase (see for

example the filament thinning measurements in [13], [14], [17] and [32]). In this case, the simple explicit expressions for the filament radius and the breakup time given in Eqs. (10) and (11) respectively can be used directly to model the capillary thinning process and determine the extensibility of the polymeric network.

8 Acknowledgements

The authors would like to thank B. Keshavarz for helpful discussions regarding filament thinning dynamics in dilute polymer solutions. CW thanks NSERC for a PGS-M Canada Graduate Scholarship (Master's Program) Award. LB thanks the MIT REED Fund for financial support of studies in the fragmentation of mucosalivary fluids. GHM would like to thank Procter & Gamble and Axalta Coating Systems for their financial support of studies in the filament thinning of complex structured fluids.

References

[1] G.H. McKinley and T. Sridhar. Filament-stretching rheometry of complex fluids. *Annual Review of Fluid Mechanics*, 34:31, 2002.

[2] A. Lindner, J. Vermant, and D. Bonn. How to obtain the elongational viscosity of dilute polymer solutions? *Physica A*, 319:9, 2003.

[3] N.F. Morrison and O.G. Harlen. Viscoelasticity in inkjet printing. *Rheologica Acta*, 49:14, 2009.

[4] S.D. Hoath, D.C. Vadillo, O.G. Harlen, C. McIlroy, N.F. Morrison, W-K. Hsiao, T.R. Tuladhar, S. Jung, G.D. Martin, and I.M. Hutchings. Inket printing of weakly elastic polymer solutions. *JNNFM*, 205:10, 2014.

[5] G. Fano. Contributo allo studio dei corpi filanti. *Archivio di fisiologia*, 5:6, 1908.

[6] L.E. Kopito and H.J. Kosasky. The tackiness rheometer determination of the viscoelasticity of cervical mucus. *Human Reproductive Medicine*, 3:11, 1979.

[7] A.V. Bazilevsky, V.M. Entov, and A.N. Rozhkov. Breakup of a liquid bridge as a method of rheological testing of biological fluids. *Fluids Dynamics*, 46:10, 2011.

[8] E. Zussman, A.L. Yarin, and R.M. Nagler. Age- and flow-dependency of salivary viscoelasticity. *Journal of Dental Research*, 86:5, 2006.

[9] A.V. Bazilevsky, V.M. Entov, and A.N. Rozhkov. Liquid filament microrheometer and some of its applications. In D.R. Oliver, editor, *Third European Rheology Conference and Golden Jubilee Meeting of the British Society of Rheology*, pages 41–43. Elsevier Science Publishers Ltd.

[10] A.V. Bazilevsky, V.M. Entov, and A.N. Rozhkov. Failure of an Oldroyd liquid bridge as a method for testing the rheological properties of polymer solutions. *Polymer Science Series A (translated from Vysokomolekulyarnya Soedineniya Seriya A pp. 474-482)*, 43:12, 2001.

[11] V.M. Entov and E.J. Hinch. Effect of a spectrum of relaxation times on the capillary thinning of a filament of elastic liquid. *JNNFM*, 72:23, 1997.

[12] G.H. McKinley. Visco-elasto-capillary thinning and break-up of complex fluids. *Rheology Reviews*, pages 1–49, 2005.

[13] R.F. Liang and M.R. Mackley. Rheological characterization of the time and strain dependence for polyisobutylene solutions. *JNNFM*, 52:19, 1994.

[14] S.L. Anna and G.H. McKinley. Elasto-capillary thinning and breakup of model elastic liquids. *Journal of Rheology*, 45:24, 2001.

[15] S.L. Anna, G.H. McKinley, D.-A. Nguyen, T. Sridhar, S.J. Muller, J. Huang, and D.F. James. An interlaboratory comparison of measurements from filament-stretching rheometers using common test fluids. *Journal of Rheology*, 45:32, 2001.

[16] C. Clasen, J.P. Plog, W.-M. Kulicke, M. Owens, C. Macosko, L.E. Scriven, M. Verani, and G.H. McKinley. How dilute are dilute solutions in extensional flows? *Journal of Rheology*, 50:33, 2006.

[17] M.D. Torres, B. Hallmark, L. Hilliou, and D.I. Wilson. Natural Giesekus fluids: shear and extensional behaviour of food gum solutions in the semi-dilute regime. *AIChE Journal*, 60:14, 2014.

[18] R.B. Bird, R.C. Armstrong, and O. Hassager. *Dynamics of Polymeric Liquids*, volume 1. John Wiley and Sons, 2nd edition, 1987.

[19] R.B. Bird, C.F. Curtiss, R.C. Armstrong, and O. Hassager. *Dynamics of Polymeric Liquids, Kinetic Theory*, volume 2. John Wiley and Sons, 2nd edition, 1987.

[20] R.B. Bird, P.J. Dotson, and N.L. Johnson. Polymer solution rheology based on a finitely extensible bead-spring chain model. *JNNFM*, 7:23, 1980.

[21] R.G. Schipper, E. Silletti, and M.H. Vinyerhoeds. Saliva as research material: Biochemical, physicochemical and practical aspects. *Archives of Oral Biology*, 52:21, 2007.

[22] L. Campo-Deaño and C. Clasen. The slow retraction method (SRM) for the determination of ultrashort relaxation times in capillary breakup extensional rheometry experiments. *JNNFM*, 165:12, 2010.

[23] D. Sachsenheimer, B. Hochstein, and N. Willenbacher. Experimental study on the capillary thinning of entangled polymer solutions. *Rheologica Acta*, 53:15, 2014.

[24] D.C. Vadillo, W. Mathues, and C. Clasen. Microsecond relaxation processes in shear and extensional flows of weakly elastic polymer solutions. *Rheologica Acta*, 51:15, 2012.

[25] A. Tripathi and G.H. McKinley. How to extract the newtonian viscosity from capillary breakup measurements in a filament rheometer. *Journal of Rheology*, 44:18, 2000.

[26] J. Eggers. Nonlinear dynamics and breakup of free-surface flows. *Reviews of Modern Physics*, 69:865, 1997.

[27] D.T. Papageorgiou. On the breakup of viscous liquid threads. *Physics of Fluids*, 7:16, 1995.

[28] A. Aggazzotti. Modificazioni della viscosita della saliva mista dopo che e'stata secreta in rapporto col potere filante e colla tensione superficiale. *Archivio di fisiologia*, 20:13, 1922.

[29] P. Szabo, G.H. McKinley, and C. Clasen. Constant force extensional rheometry of polymer soutions. *JNNFM*, 169-170:15, 2012.

[30] G. Lielens, R. Keunings, and V. Legat. The FENE-L and FENE-LS closure approximations to the kinetic theory of finitely extensible dumbbells. *JNNFM*, 87:20, 1999.

[31] M.S.N. Oliveira, R. Yeh, and G.H. McKinley. Iterated stretching, extensional rheology and formation of beads-on-a-string structures in polymer solutions. *JNNFM*, 137:12, 2006.

[32] S.J. Haward, V. Sharma, C.P. Butts, G.H. McKinley, and S.S. Rahatekar. Shear and extensional rheology of cellulose/ionic liquid solutions. *Biomacromolecules*, 13:12, 2011.